

# The Concordance Cosmic Star Formation Rate: Implications from and for the Supernova Neutrino and Gamma Ray Backgrounds

Louis E. Strigari<sup>1</sup>, John F. Beacom<sup>1,2</sup>, Terry P. Walker<sup>1,2</sup>, and  
Pengjie Zhang<sup>3</sup>

<sup>1</sup>Department of Physics, The Ohio State University, Columbus, OH 43210

<sup>2</sup>Department of Astronomy, The Ohio State University, Columbus, OH 43210

<sup>3</sup>NASA/Fermilab Astrophysics Center, Fermi National Accelerator Laboratory,  
Batavia, IL 60510-0500

E-mail: strigari@mps.ohio-state.edu, beacom@mps.ohio-state.edu,  
twalker@mps.ohio-state.edu, zhangpj@fnal.gov

**Abstract.** We constrain the Cosmic Star Formation Rate (CSFR) by requiring that massive stars produce the observed UV, optical, and IR light while at the same time not overproduce the Diffuse Supernova Neutrino Background as bounded by Super-Kamiokande. With the massive star component so constrained we then show that a reasonable choice of stellar Initial Mass Function and other parameters results in SNIa rates and iron yields in good agreement with data. In this way we define a ‘concordance’ CSFR that predicts the optical SNII rate and the SNIa contribution to the MeV Cosmic Gamma-Ray Background. The CSFR constrained to reproduce these and other proxies of intermediate and massive star formation is more clearly delineated than if it were measured by any one technique and has the following testable consequences: (1) SNIa contribute only a small fraction of the MeV Cosmic Gamma-Ray Background, (2) massive star core-collapse is nearly always accompanied by a successful optical SNII, and (3) the Diffuse Supernova Neutrino Background is tantalizingly close to detectability.

## 1. Introduction

The Cosmic Star Formation Rate (CSFR), which encodes the history of stellar birth, life, and death, is an essential probe of the evolution of galaxies and the Universe. In recent years, the CSFR has been probed out to redshifts  $z \sim 6$ , the results all indicating that the CSFR was nearly an order of magnitude greater in the past than today [1–11]. The CSFR is often measured by the total light output from young, bright stars, though this can be significantly complicated by dust obscuration. One can also probe the CSFR with the by-products of stellar death: e.g., the neutrinos from core-collapse Type II supernovae (SNII) for massive stars, and gamma rays from Type Ia supernovae (SNIa) for some stars of intermediate mass.

Each SNII event creates a prompt burst of  $10^{58}$  neutrinos, a result which was confirmed by the detection of the neutrino flux from SN 1987A in the Large Magellanic Cloud [12, 13]. Though the neutrino flux from an individual SNII beyond the local group of galaxies is below the threshold of current detectors [14], the cumulative emission from all past SNII results in a *Diffuse Supernova Neutrino Background* (DSNB), which is on the verge of detectability. Though the search for the DSNB flux is hindered by atmospheric neutrino backgrounds, Super-Kamiokande has established an upper limit on the electron anti-neutrino flux above 19.3 MeV of  $1.2 \text{ cm}^{-2} \text{ s}^{-1}$  [15], which nearly agrees with recent theoretical predictions [16–18]. The DSNB flux probes the history of the SNII rate, about which little is directly known, both locally and at high redshifts. Therefore, observations of the high mass CSFR, corresponding to the range of SNII progenitors, are generally used in predictions for the DSNB flux. The Super-Kamiokande flux limit is in fact strict enough to rule out scenarios for the CSFR, and provides a strong limit on the dust corrections applied to UV light measurements.

By combining the DSNB flux limit with determinations of the CSFR from light surveys and other data, we construct a more restrictive concordance model for the CSFR. More specifically, the DSNB sets an upper limit on the cosmic SNII rate, and therefore the CSFR above the core-collapse threshold mass of  $8 M_{\odot}$  [19]. Throughout this paper, we follow the convention of referring to massive star core-collapse generically as SNII, including the less dominant core-collapse SNIb and SNIc in this definition. We assume these stars end their lives in a prompt burst of neutrinos. Generally, massive star core-collapse need not produce visible light, if the core bounce shock fails to eject the stellar envelope and a black hole is formed [19–21]. When the supernova is successful, we refer to it as an optical SNII. The massive stars which emit UV light in their lifetimes also contribute to the cosmic far infrared background (FIRB) flux, which is believed to arise from the absorption and re-emission of UV light [22, 23]. Measurement of the slope of the CSFR from UV and IR light, combined with a normalization from the DSNB flux, provides a tight constraint on the CSFR for  $M > 8 M_{\odot}$  and  $z \lesssim 1$ .

We determine the intermediate-mass CSFR from the high-mass CSFR using the stellar *Initial Mass Function* (IMF), which is observed to have a universal slope above  $\sim 0.5 M_{\odot}$ . The intermediate-mass ( $\sim 3 - 8 M_{\odot}$ ) CSFR has implications for the rate of

SNIa, though knowledge of the IMF and high mass CSFR does not precisely fix the SNIa rate. The lack of a well-defined progenitor model introduces some ambiguity in the time delay between progenitor formation and explosion, and the efficiency for creating SNIa from a main sequence population. However, these parameters can be fixed empirically by requiring a progenitor model to reproduce the observed evolution of the SNIa rate and the contribution to the mean iron abundance in the universe. We examine a range of allowed values for these parameters, and use these to examine the evolution of the SNIa rate.

Each SNIa event is expected to produce  $\sim 10^{55}$  gamma rays, and thus the SNIa rate can be tested by the SNIa contribution to the MeV *Cosmic Gamma-Ray Background* (CGB). From the hard x-rays to high energy gamma rays, the CGB spectrum is observed to have a steep decline, and is typically explained as the sum of three components. Unresolved active galaxies are believed to be the dominant sources below  $\sim 1$  MeV (Seyferts) and above  $\sim 10$  MeV (Blazars). These hypotheses are strengthened by the fact that observations of resolved Seyferts and Blazars, combined with estimates of their number density, can reasonably reproduce the spectrum normalization and shape in the respective energy ranges [24]. In the range 1–3 MeV, it has generally been assumed that SNIa account for the measured CGB [25–28]. In this paper we show that the derived limits on the SNIa rate implies that SNIa cannot be the principal source of the MeV CGB.

The paper is organized as follows. In Section 2 we review current observations for the CSFR. In Section 3 we discuss the relation between the SNII rate and the DSNB. In Section 4, we estimate the evolution of the supernova rates, and in Section 5 we discuss estimates of the iron abundance and the far infrared background. In Section 6 we use the SNIa rate to estimate the SNIa contribution to the CGB, and in Section 7 we discuss some implications for the DSNB and the CGB.

## 2. The Concordance Cosmic Star Formation Rate

Determining the CSFR at a particular redshift typically involves either measuring a UV continuum or  $H\alpha$  emission for a particular galaxy, and then multiplying by the space density of galaxies at that redshift [29]. These results depend most strongly on stars of mass  $\gtrsim 3 M_{\odot}$ , and require extrapolation of the IMF to lower masses to obtain the CSFR for all masses. The corrections for UV extinction by dust are large, and at least until recently, rather uncertain.

Complementing these methods are recent results from the 2-degree Field survey (2dF) and Sloan Digital Sky Survey (SDSS), which measure the ensemble spectrum of present day galaxies, thus determining the mix of old and young stellar populations and fitting CSFR models to this spectrum [30, 31]. These results are sensitive to the entire range of stellar masses, and thus have a different (and ideally less strong) dependence on the assumed dust extinction corrections. Given the limitations of existing data, in the analysis of the 2dF and SDSS cosmic optical spectrum, the CSFR was parametrized

as a broken power law:

$$\begin{aligned} R_{\text{SF}}(z) &= R_{\text{SF}}(0)(1+z)^\beta \quad \text{for } z < z_p \\ &= R_{\text{SF}}(z_p)(1+z)^\alpha \quad \text{for } z > z_p, \end{aligned} \quad (1)$$

where  $\beta \sim 2$ ,  $z_p \sim 1 - 2$  is the transition redshift, and  $\alpha \sim 0$ .

In Figure 1, we show representative fits to observations of the CSFR. The entire cross-hatched plus shaded region depicts the allowed region from the 2dF and SDSS cosmic optical spectrum. For  $z < 1$ , the upper curve has  $\beta = 4$ , and the lower curve has  $\beta = 2$ . For both the upper and lower limits we use  $\alpha = 0$  beyond  $z_p = 1$ ; both  $\alpha$  and  $z_p$  are quite uncertain from this data alone. As examples of very recent UV measurements, we show lines corresponding to the results of Cole et al. [34], Dahlen et al. [32, 35], and GALEX [33]. All three results are corrected for dust extinction by the authors; after correction, these UV results are consistent with  $\text{H}\alpha$  results. We show also the uncorrected results of Cole et al. [34] as an example, as the corrections of the other authors are similar.

The limit on the neutrino flux from the core collapse of massive stars provides an important upper bound on the CSFR. We emphasize that this is an *integral* constraint, and does not provide *differential* sensitivity to the CSFR at each redshift. Nevertheless, it is a strong constraint. Following the 2dF and SDSS analysis, we adopt the above four-parameter form for the CSFR. Since there is little sensitivity beyond  $z \gtrsim 1$ , we conservatively fix  $z_p = 1$  and  $\alpha = 0$  (in Figure 1 we show redshifts up to  $z = 2$  for illustration; less than 5% of the DSNB flux in the observable Super-K energy range comes from  $z > 1$ ). Further, the UV and  $\text{H}\alpha$  results do constrain  $\beta$  well, so we fix  $\beta = 2$  (choosing  $\beta$  on the small side gives a more conservative limit on the normalization). What remains is  $R_{\text{SF}}(0)$ , and the DSNB limit on this quantity is completely independent of the issues associated with dust extinction.

The interesting tension is between the recent UV data, which has in recent analyses been rising in normalization, and the DSNB limit, which does not allow any further increase. In fact, as we discuss below, these dust corrected models are marginally inconsistent with the DSNB upper limit; however, we view this discrepancy as within the uncertainties. Though the 2dF and SDSS band includes a region below the dust corrected models, it is disfavored by combining all data sets. The concordance region is concentrated around the DSNB upper limit, consistent with the light output of massive stars. Thus the ‘‘concordance’’ CSFR we obtain is principally defined by the upper limit on the normalization  $R_{\text{SF}}(0) \simeq 2 \times 10^{-2} M_\odot \text{ yr}^{-1} \text{ Mpc}^{-3}$  (with the assumed redshift dependence of the CSFR). On the other hand, recent astronomical data probably do not permit a normalization below  $R_{\text{SF}}(0) \simeq 1 \times 10^{-2} M_\odot \text{ yr}^{-1} \text{ Mpc}^{-3}$ . While the existing data do not warrant a more sophisticated statistical analysis, it is clear that these combined results are much more constraining than those of any one technique alone.

We use the results from Figure 1 to estimate the supernova rates, placing a strong focus on  $z \lesssim 1$ , which is the most relevant range for the supernova neutrino and gamma ray backgrounds. That is, in later figures the shaded bands shown correspond exactly

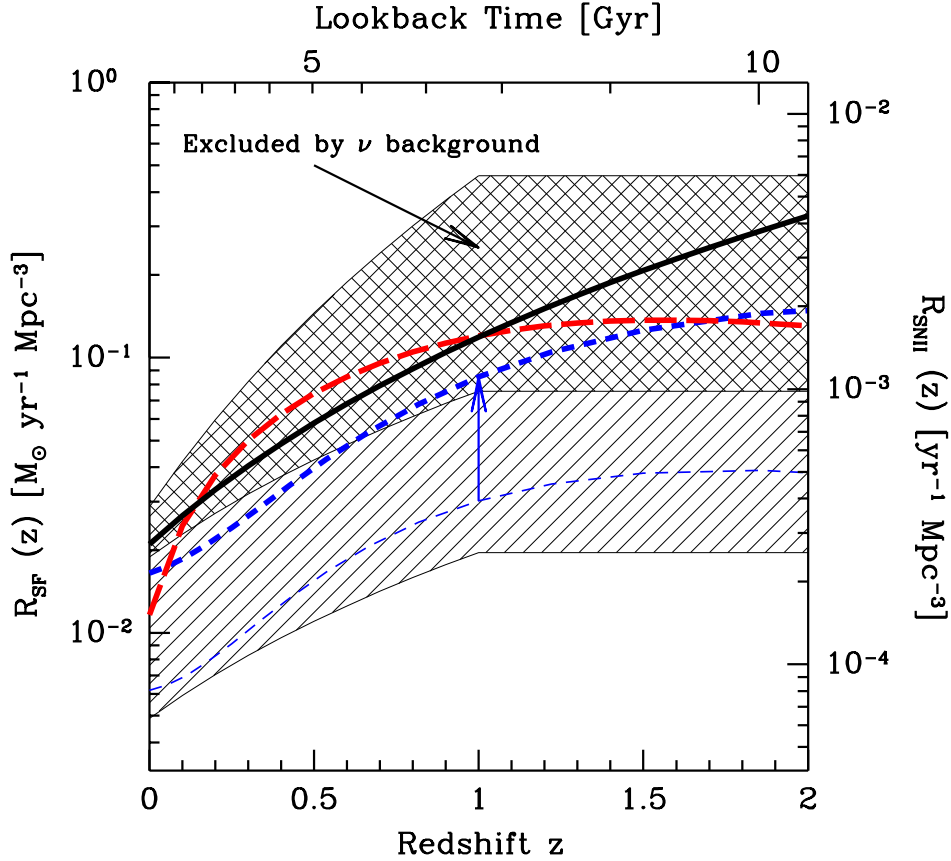


**Figure 1.** Observational results for the Cosmic Star Formation Rate, with the conversion to SNII rate on the right axis using Equation (4). The entire cross-hatched plus shaded region is consistent with the results of the 2dF and SDSS cosmic optical spectrum [30, 31]. The upper cross-hatched region is ruled out by the limit on the DSNB flux, while the lower shaded region is allowed. Three recent (dust corrected by those authors) results are also shown: long-dashed red line (Dahlen et al. [32]), solid black line (GALEX [33]), and short-dashed blue line (Cole et al. [34]). In the latter case we also show their result before dust correction [34]; dust corrections in the other cases are similar. The concordance region is driven by the proximity of these recent observations to the upper bound from the neutrino data, and therefore is concentrated at the upper edge of the lower band.

to the lower shaded band in Figure 1; the region shown with the cross-hatched band in Figure 1 is considered excluded by the DSNB limit. Furthermore, as noted by our approximate constraint on  $R_{\text{SF}}(0)$ , the upper part of each shaded region is preferred.

### 3. The SNII Rate and the Diffuse Supernova Neutrino Background

Though the CSFR is observationally well-studied, relatively little is known about the optical SNII rate, even locally. The high mass and short lifetimes of the progenitor stars

imply that the SNII rate is directly proportional to the CSFR at the same epoch. The DSNB has been the subject of many previous studies, most recently in [16–18, 36] (for earlier predictions, see [37–47], and for a recent review, see [48]). In this section, we review current estimations for the DSNB flux, updating for new results for the CSFR. For more details on the flux calculation we refer to Strigari et al. [18].

The DSNB flux is a convolution of the SNII rate with the neutrino emission spectrum. We denote the supernova rate as a function of redshift as  $R_{\text{SNII}}(z)$  (in units of number of supernovae per time per comoving volume), and the neutrino spectrum from an individual SNII event as  $dN/dE$ . The number flux of neutrinos from SNII events is  $4\pi n$  (using  $c = 1$  here and elsewhere), where  $n$  is the comoving neutrino number density, and the differential flux in units of number of neutrinos per time  $t$ , per area  $A$ , per energy is

$$\frac{dN}{dt dA dE} = \int_0^{z_{\text{max}}} R_{\text{SNII}}(z) \frac{dN(E(1+z))}{dE} (1+z) \left| \frac{dt}{dz} \right| dz. \quad (2)$$

Here  $E(1+z)$  is the neutrino energy at emission,  $E$  is the energy at detection, and  $z_{\text{max}}$  is the redshift at which star formation begins. Here we take  $z_{\text{max}} = 5$ , though our results are insensitive to this choice. We use a flat  $\Lambda$ CDM cosmology, with  $\Omega_{\text{M}} = 0.3$  and  $H_0 = 70 \text{ km s}^{-1} \text{ Mpc}^{-1}$  [49], giving

$$\left| \frac{dt}{dz} \right| = \frac{1}{H_0(1+z) \sqrt{\Omega_{\text{M}}(1+z)^3 + \Omega_{\Lambda}}}. \quad (3)$$

The DSNB flux thus depends primarily on the SNII neutrino spectrum and the SNII rate as a function of redshift. In a SNII event, all flavors of neutrinos are created with thermal spectra. Each neutrino flavor is characterized by a temperature which depends on the radius at which the neutrino decouples from the matter in the interior of the proto-neutron star (for recent results on flavor dependent neutrino fluxes from SNII, see [50]). SNII produce an order of magnitude fewer gamma rays than SNIa, and they are attenuated further by the thick stellar envelope.

The Super-Kamiokande upper limit on the flux of DSNB electron antineutrinos above 19.3 MeV is  $1.2 \text{ cm}^{-2} \text{ s}^{-1}$ . This is based on the limit on the rate of positron-like events caused by DSNB neutrinos undergoing  $\bar{\nu}_e + p \rightarrow e^+ + n$  [15]. As discussed in the previous section, we use this integral constraint on the CSFR to bound  $R_{\text{SF}}(0)$ .

Converting the CSFR from Equation 1 to the SNII rate requires the IMF. The IMF as measured in different environments is consistent with a power law,  $dn/dm \propto m^{-2.35}$ , in the range  $m > 0.5 M_{\odot}$ . The SNII rate as a function of redshift is then

$$R_{\text{SNII}}(z) = \int_8^{30} \frac{dn}{dm} R_{\text{SF}}(z) dm, \quad (4)$$

where the units of mass are  $M_{\odot}$ . Here  $dn/dm$  is the normalized IMF, where for masses less than  $0.5 M_{\odot}$  we are using a slope  $m^{-1.50}$  [51]. We impose an upper cut-off to the integral of  $30 M_{\odot}$ , though our results are insensitive to this choice. Thus  $\sim 1\%$  of all stellar mass becomes core-collapse supernovae. In Figure 2 we show the range of allowed DSNB spectra, corresponding to the allowed region in Figure 1.

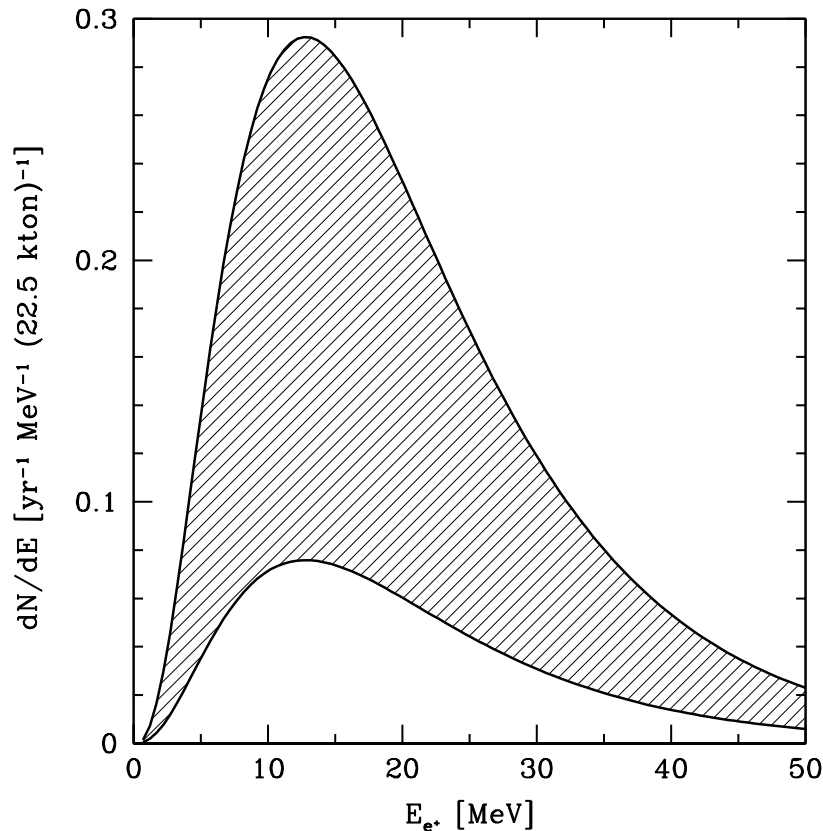


**Figure 2.** The DSNB detection spectrum at Super-Kamiokande (i.e., weighted by the detection cross section for  $\bar{\nu}_e + p \rightarrow e^+ + n$ ). The shaded region shown corresponds to the similarly shaded region in Figure 1. The upper limit is determined by the Super-Kamiokande bound, and the lower limit by the 2dF and SDSS data. As noted, in the concordance model, the upper edge of the region is favored. There are significant detector backgrounds, which are discussed in [16, 18, 36].

#### 4. The Type Ia Supernova Rate

SNIa are believed to result from the thermonuclear detonation of a white dwarf that has accreted the outer layer of its companion star to the instability point. In this model, the main sequence lifetime of the progenitor star, combined with the accretion rate of the white dwarf from the giant companion, imply a  $\sim$  Gyr delay time between star formation and the SNIa event. This time delay implies a different relationship between the CSFR and SNIa rate compared to the relation between the CSFR and the SNII rate. The result is that the SNIa rate at a fixed redshift is an indirect tracer of the CSFR at earlier epochs.

Additionally, SNIa result from a lower mass range of the stellar IMF, approximately  $3 - 8 M_{\odot}$  [52]. The shape of the IMF provides more stellar mass in this range relative to the range for SNII progenitors, but SNIa are observed to be several times more rare than their SNII counterparts, both locally and at moderate redshifts. This result implies

that the efficiency for creating SNIa is less than that for SNII, which are expected to have an efficiency factor near unity for stars greater than  $8 M_{\odot}$  (see discussion below).

We parametrize the SNIa rate as

$$R_{\text{SNIa}}(t) = \eta \int_3^8 dm \frac{dn}{dm} \int_0^t dt_{Ia} R_{\text{SF}}(t - t_{Ia}) g(t_{Ia}). \quad (5)$$

Here  $t_{Ia}$  is the delay time and  $\eta \sim 1\%$  is the efficiency of producing an SNIa event from stellar mass in the range  $3 - 8 M_{\odot}$ . The delay time has been previously estimated by comparing the observed CSFR to the SNIa rate as a function of redshift [35, 53, 54], or from chemical evolution models comparing the observed element enrichment as a function of redshift [55]. These results indicate mean time delays roughly in the range  $1 - 3$  Gyr. With the current data on the SNIa rate, models with a constant time delay are not distinguishable from more complicated models [54]. Here we consider a constant time delay of 3 Gyr, i.e.  $g(t_{Ia}) = \delta(t_{Ia} - 3 \text{ Gyr})$ , independent as well of the mass of the progenitor star.

For this fixed time delay, we determine  $\eta$  by comparing the observed CSFR to the SNIa rate, and make the replacement in Equation 5 that  $\eta dn/dm \rightarrow f_{Ia}$ . This approach was taken by Ruiz-Lapuente et al. [27], in comparing the SNIa rate to  $R_{\text{SF}}(z)$  at different redshifts. We additionally apply the constraint on the CSFR above  $8 M_{\odot}$  (or equivalently  $R_{\text{SNII}}(z = 0)$ ) from the DSNB flux. Given the values of  $\beta$  and  $R_{\text{SNII}}(z = 0)$  that maximize the DSNB flux, and a fixed time delay of 3 Gyr, we determine that  $f_{Ia} = (1/700 - 1/1000) M_{\odot}^{-1}$  in order to remain consistent with the results for the SNIa rate evolution. Motivated by establishing a robust upper limit to the SNIa CGB flux below, we choose  $(1/700) M_{\odot}^{-1}$ .

In Figure 3, we show our limits for the evolution of the supernova rates in comparison to the observational results. The allowed bands for the SNII and SNIa bands are correlated, in the sense that increasing the SNIa contribution by increasing  $R_{\text{SF}}(z = 0)$  implies a similar increase in the SNII contribution, which would violate the DSNB flux limit. For this figure we have used  $R_{\text{SF}}(z = 0) = 1.9 \times 10^{-2} M_{\odot} \text{ yr}^{-1} \text{ Mpc}^{-3}$  and  $\beta = 2$ .

Below we consider the CGB as an observable test of the SNIa rate. Though changing the slope to  $\beta = 4$  would require lowering  $R_{\text{SNII}}(z = 0)$  to remain consistent with the DSNB flux limit, this does not appreciably change the SNIa CGB flux in the detectable energy range  $0.8 - 3.0$  MeV. For a CSFR that increases or remains constant beyond  $z \sim 1$ , the 3 Gyr time delay gives a maximal contribution to the observable SNIa CGB flux. When considering a fixed value for  $R_{\text{SNIa}}(z = 0)$ , the time delay is degenerate with the value of  $f_{Ia}$ , such that an increase in the time delay requires a decrease in  $f_{Ia}$ . This results from the fact that greater time delays sample the CSFR at higher redshifts.



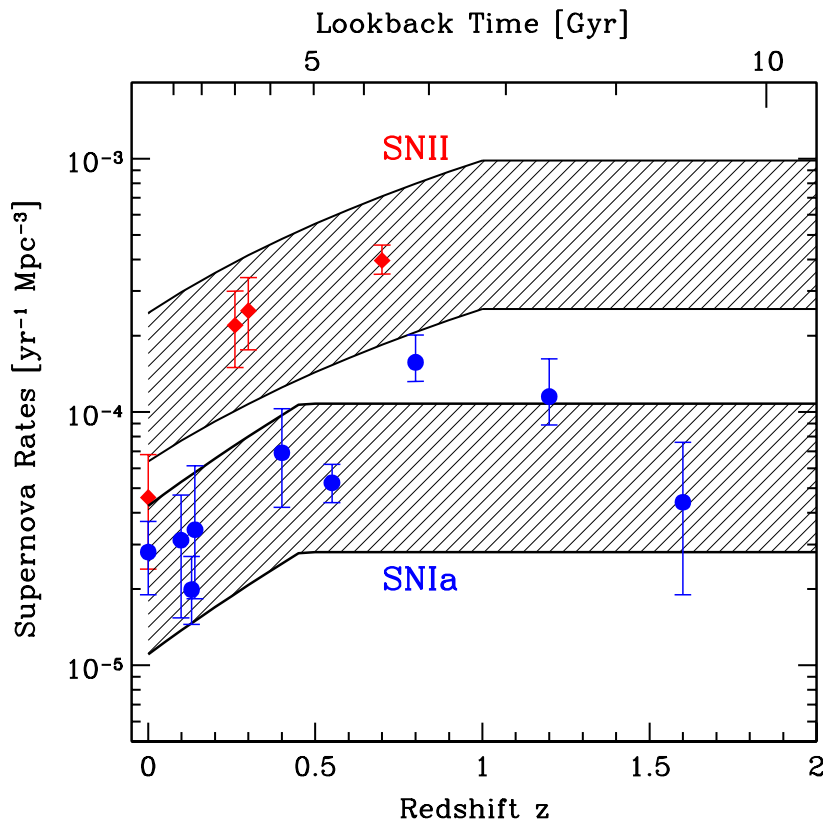


**Figure 3.** The allowed bands for the supernova rates follow from the lower allowed band of Figure 1. The SNIa data is from [32] and [56], and the optical SNII data is from [32] and [57]. The error bars show statistical uncertainties. As discussed in Cappellaro et al. [57], the  $z = 0$  optical SNII measurement is not corrected for dust extinction, and represents a lower limit. For the SNIa calculations, we use  $f_{Ia} = (1/700) M_{\odot}^{-1}$  and a time delay of 3 Gyr.

## 5. The Iron Abundance and Far IR Background

### 5.1. Iron Abundance

Observations and models indicate that, on a per event basis, SNIa produce an order of magnitude more iron than SNII [58]. With the concordance CSFR, the integrated SNII number density is roughly an order of magnitude greater than that for SNIa (Figure 3). The net result is that each type of supernova is expected to produce roughly half of the observed  $^{56}\text{Fe}$ . With a parametrization for the supernova rates as a function of redshift, and the mean amount of  $^{56}\text{Ni}$  produced for each type of supernova, we can compare the expected supernova yields to the observed  $^{56}\text{Fe}$  abundances. Renzini [59] has compiled measurements of  $^{56}\text{Fe}$  abundances in the intracluster medium of galaxy groups and clusters, with an approximate average abundance of 30% solar by mass fraction. Additionally, studies of the  $^{56}\text{Fe}$  abundance in Damped Lyman-alpha systems show a large scatter in  $[\text{Fe}/\text{H}]$ , with a upper limit of roughly  $10^{-3}$  as a fraction of the total

baryonic mass [60]. Given the difficulty in measuring the  $^{56}\text{Fe}$  abundance, a comparison between the observed yields and that expected to be contributed from supernovae is not very precise. Nevertheless, assuming the current data for  $^{56}\text{Fe}$  cluster abundances to represent the average abundance in the  $z = 0$  universe [59], the observed  $^{56}\text{Fe}$  density parameter is

$$\Omega_{\text{Fe,Obs}} = 0.3 Z_{\odot} \Omega_b \simeq 2 \times 10^{-5}, \quad (6)$$

with  $Z_{\odot} = 0.0013$  the solar system  $^{56}\text{Fe}$  mass fraction [61]. For SNII, integrating the upper limit curve in Figure 3 to obtain the total comoving number density of SNII, and an average  $^{56}\text{Ni}$  production per event of  $0.06 M_{\odot}$ , the amount of  $^{56}\text{Fe}$  contributed by SNII is  $\Omega_{\text{Fe,SNII}} \simeq 0.6 \times 10^{-5}$ . Similarly, from the upper limit SNIa curve as constrained by the DSNB, and with  $0.5 M_{\odot}$  per SNIa event the  $^{56}\text{Fe}$  contribution is  $\Omega_{\text{Fe,SNIa}} = 0.4 \times 10^{-5}$ . Thus in our concordance model, the predicted  $^{56}\text{Fe}$  yield from SNII plus SNIa is within a factor of two of the data, precluding the possibilities that either supernova rate is significantly larger, or that both are significantly smaller. More precise measurements of  $^{56}\text{Fe}$  abundances at all redshifts, when combined with tighter constraints on the  $^{56}\text{Fe}$  production per event, will strengthen the constraints on the supernova  $^{56}\text{Fe}$  production. Still, the existing crude constraint provides additional evidence to support our concordance model.

### 5.2. The Cosmic Far IR background

While stars with mass greater than  $8 M_{\odot}$  produce the DSNB flux, the cosmic far infrared background flux is dominated by the absorption of UV light on dust and re-emission at longer wavelengths from all massive stars, making the observation of the FIRB flux limits an independent determination of the CSFR in this stellar mass range. This mass range is the same as that probed by SNIa, as well as by massive x-ray binary systems [62], and therefore the CSFR as constrained by each of these proxies should be in agreement. The detailed analysis of the reprocessed starlight which accounts for the FIRB will involve modeling the evolution of dust components and temperature at all redshifts (e.g., [63]). The observed FIRB intensity ( $\gtrsim 100 \mu\text{m}$ ) is  $I_{\nu} \sim 30 \text{ nw m}^{-2}\text{sr}^{-1}$  [23], a result which is still subject to systematic errors from foreground contaminations [22, 23]. With reasonable assumptions for the dust, the FIRB intensity is reproduced with a CSFR similar to those measured by UV surveys, and so is consistent with the concordance model presented here [33]. In coming years the FIRB will be mapped by Spitzer from the near to far IR, giving constraints on the CSFR as well as the population of IR galaxies at high redshift [64].

## 6. The Cosmic Gamma-Ray Background

In previous sections we have developed a concordance model of the CSFR as constrained by the DSNB and light surveys, and from this predicted the expected ranges for the evolution of supernova rates and other indicators. Next we use our results to calculate

the portion of the MeV CGB made by SNIa. The connection between the DSNB and CGB has been previously discussed by Hartmann et al. [65] and by Zhang and Beacom [28]. Additionally, Buonanno et al. [66] have recently explored the connections between the neutrino and gravitational wave backgrounds, providing an initial estimate of the expected gravitational wave background from core-collapse supernovae.

### 6.1. The CGB data

The CGB has been measured by the Solar Maximum Mission (SMM) in the energy range 0.3 – 7 MeV [67] and the Compton imaging telescope COMPTEL in the energy range 0.8 – 30 MeV [68, 69]. The CGB analysis is hindered by instrumental and cosmic-ray backgrounds, which must be carefully subtracted to reveal the underlying signal. Below 100 keV and above 10 MeV, the diffuse background is expected to result from the addition of individual unresolved point sources, with Seyfert galaxies dominating at low energies and EGRET-detected Blazars contributing at high energies. Radio-loud Seyferts, such as Centarus A, are observed with spectra that continue beyond 100 keV, though the present density of such sources, combined with the extrapolation of the spectrum tail to 10 MeV, do not imply a large contribution to the diffuse background [70]. Additionally, the Blazar spectra detected by EGRET, and confirmed by COMPTEL at lower energies, implies a spectrum break and flux suppression below 10 MeV, likely ruling out significant contribution to the MeV background [71] (however, two AGN detected by EGRET and confirmed by COMPTEL are exceptionally bright and time-varying sources at 1 – 10 MeV [72]).

In the energy range 0.8 – 30 MeV, the CGB spectrum fit by COMPTEL is [69]

$$\frac{dN}{dt dA dE d\Omega} = (1.1 \pm 0.2) \times 10^{-4} \left( \frac{E}{5 \text{ MeV}} \right)^{-2.4 \pm 0.2} (\text{MeV}^{-1} \text{cm}^{-2} \text{s}^{-1} \text{sr}^{-1}). \quad (7)$$

This data is consistent, within large uncertainties, with a low energy extrapolation from the EGRET background spectrum and high energy extrapolation of the SMM spectrum, with an evolution from harder to softer spectrum in the COMPTEL range. It has been commonly accepted that SNIa provide the primary contribution to the CGB in 0.8 – 3 MeV [25–28]. In the remaining parts of this section we test this hypothesis.

### 6.2. The SNIa Gamma Ray Spectrum

During the thermonuclear explosion of a SNIa,  $^{56}\text{Ni}$  is produced as the nuclear burning wave propagates through the white dwarf core. This subsequently decays (half life  $\sim 6$  days) to  $^{56}\text{Co}$  and then (half life  $\sim 77$  days) to stable  $^{56}\text{Fe}$ ; these decays are often to nuclear excited states, and are thus accompanied by MeV gamma rays. Most gamma rays from  $^{56}\text{Ni}$  are unable to escape from the dense environment and are degraded into x-ray and lower energies. As the optical light curve declines, the thinning outer layers are expected to become optically transparent to gamma rays from the decay of  $^{56}\text{Co}$ . In total, SNIa are expected to produce  $\sim 0.5 M_{\odot}$  of  $^{56}\text{Ni}$ , with exact mass depending on the nature of the nucleosynthesis in the core.

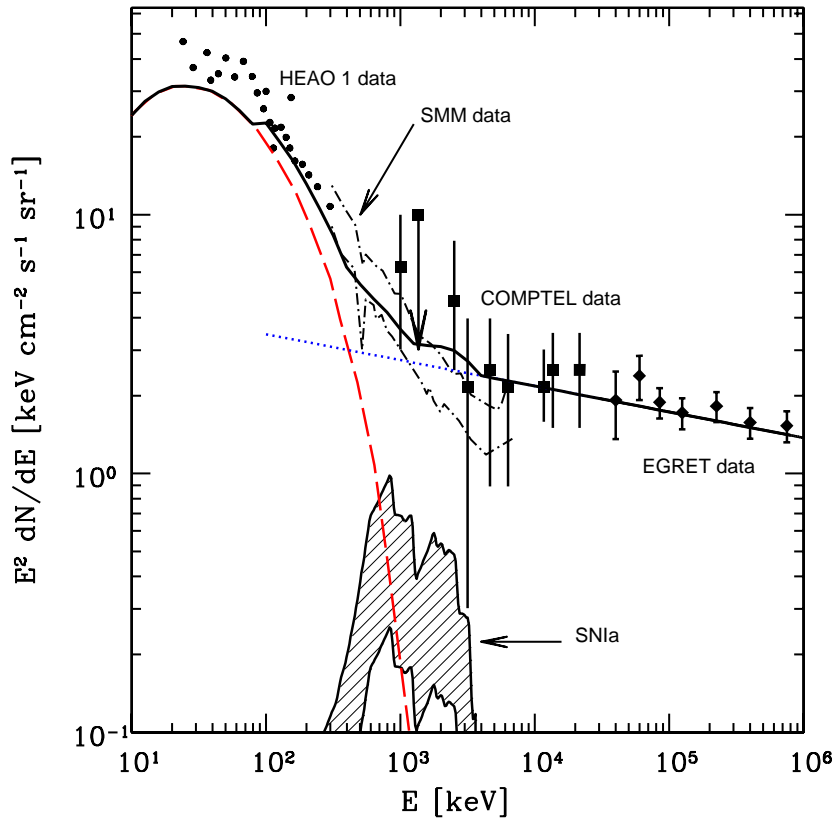


**Figure 4.** The observational results for the CGB spectrum with the shading corresponding to the previous figures. The band shows the allowed contribution from SNIa, with the upper edge of the band preferred in our concordance model. The data from COMPTEL are shown as squares [68], and SMM data range is given by the two dash-dotted lines [67]. Also shown are the HEAO x-ray data (circles) [73], and the EGRET data (diamonds) [74]. The blue dotted line is the power law fit to the EGRET background and our assumed low energy extrapolation, and the red dashed curve is the expected contribution to the x-ray background from Seyfert galaxies [75]. The bold black curve is the sum of the Seyfert, SNIa, and Blazar spectra, with our assumed low energy extrapolation.

The SNIa gamma ray spectrum is thus characterized by lines which encode the competition between the strength of the flux from  $^{56}\text{Ni}$  and  $^{56}\text{Co}$  decays, and the opacity of the stellar material to gamma rays. In our calculations we use the standard W7 model of Nomoto et al. [76], as presented in Watanabe et al. [26], for a representative spectrum. The normalization of this spectrum is such that an average SNIa produces  $0.5 M_{\odot}$  of  $^{56}\text{Ni}$ , corresponding to  $1.1 \times 10^{55}$  gamma rays. Long-lived radioactive isotopes, such as  $^{44}\text{Ti}$ ,  $^{26}\text{Al}$ ,  $^{60}\text{Co}$ , as well as positrons contribute to the gamma ray flux, though at a level less by a few orders of magnitude.

Three nearby SNIa have been studied in gamma rays, resulting in upper limits on the gamma ray flux  $\sim 10^{-5} \text{ cm}^{-2} \text{ s}^{-1}$  for a SNIa at an assumed distance of 10 Mpc [77].

These observed limits are very near theoretical flux predictions, leading to constraints on the mass of  $^{56}\text{Ni}$  produced in SNIa, and are consistent with our normalization of the spectrum. These results indicate that the gamma ray emission from SNIa is not *larger* than assumed here.

### 6.3. The SNIa Contribution to the CGB

The SNIa contribution to the CGB flux is determined directly from the SNIa gamma ray spectrum and the SNIa rate. The SNIa CGB flux is given by Equation (2), after accounting for the convention that the CGB flux is typically quoted per solid angle. The shape of the SNIa CGB is determined primarily by the decay lines of  $^{56}\text{Ni}$  and  $^{56}\text{Co}$ . The spectrum cuts off above 3 MeV, since the radioactive decay of these isotopes do not emit gamma rays above that energy. At energies below 1 MeV, the spectrum blends into a hard x-ray continuum below the threshold for gamma ray telescopes. The spectral features from the decay of  $^{56}\text{Ni}$  and  $^{56}\text{Co}$  are smoothed out by integration over the SNIa redshifts, though these features could be recovered by considering the angular correlations of the CGB flux [28].

In Figure 4 we show the SNIa CGB spectrum, with a range determined by the uncertainty in the SNIa rate from Figure 3. The parameters for the SNIa rate have been chosen as in Section 4. We have determined a firm upper limit to the normalization on the SNIa CGB from the concordance CSFR, and this upper limit is nearly an order of magnitude below the CGB data. If SNIa had been the dominant source in the MeV range, spectral breaks might have been seen, marking the transitions to other sources at lower and higher energies. While the data can exclude strong breaks, more mild transitions cannot be ruled out from the data alone. Here we have used strong and independent evidence to exclude a significant SNIa contribution to the MeV CGB. Still, a small and possibly detectable contribution from SNIa may remain (see Figure 4).

### 6.4. Comparison to Previous Results

The SNIa contribution to the CGB has been studied by previous authors. Ruiz-Lapuente et al. [27] compare the evolution of the SNIa rate with CSFR models to conclude that reasonable models exist in which the CGB can be fully accounted for by the SNIa contribution. The analysis of Watanabe et al. [26] concludes that SNIa may not be able to account for the entire CGB, but uncertainties on  $R_{\text{SF}}(z=0)$  at that time prevented them from drawing stronger conclusions. Zhang and Beacom [28] focused on angular correlations of the CGB, and normalized their diffuse SNIa spectrum to match the COMPTEL data.

Given that these previous calculations use similar SNIa spectra based on the models of Nomoto et al. [76], the primary difference in these results is the adopted CSFR. With a 1 Gyr delay time,  $\Lambda$ CDM cosmology, peak redshift of star formation at  $z=1$ , and a normalization of the SN rates such that  $R_{\text{SNIa}}/R_{\text{SNII}} = 1/3$ , Watanabe et al. obtain a present SNIa rate of  $R_{\text{SNIa}}(z=0) = 6 \times 10^{-5} \text{ yr}^{-1} \text{ Mpc}^{-3}$ . With 3 Gyr delay

normalization to the SNII neutrino limit, and efficiency determined from the evolution of the SNIa rate, we obtain  $R_{\text{SNIa}}(z=0) = 3 \times 10^{-5} \text{ yr}^{-1} \text{ Mpc}^{-3}$ . Ruiz-Lapuente et al. scan the space of allowed range for the CSFR, but appear to have overestimated the SNIa gamma ray spectrum by an order of magnitude (Figure 3 of [27]), leading them to conclude that the MeV CGB is entirely from SNIa. In this paper we show, even with the maximum allowed CSFR, that the MeV CGB cannot be of SNIa origin.

## 7. Discussion and Conclusions

### 7.1. New Sources for the Cosmic Gamma-Ray Background

Knowledge of the SNIa rates gives the best prediction yet for the SNIa contribution to the MeV CGB. With the SNIa rate which we have determined, we can limit the observed SNIa contribution to the CGB to nearly an order of magnitude less than observed. Here we consider the robustness of this estimate. Our CSFR, as constrained by the DSNB, reproduces the observed SNIa rate with reasonable choices of the SNIa efficiency and time delay. Our DSNB-constrained CSFR and SNIa formation scenario is also in good agreement with a variety of constraints on the light and Fe generated by stars of intermediate mass and larger. In this sense, we have deemed this model ‘concordance.’

In our analysis, the SNIa gamma ray luminosity assumed is the maximum allowed by constraints from observations of individual SNIa [32]. Keeping the gamma ray luminosities fixed, could it be that SNIa are 10 times more abundant, either because they form more efficiently and/or because the intermediate mass CSFR is larger than we derive here? Either of these possibilities would mean that the SNIa are ten times more frequent than surveys indicate and that the iron produced per SNIa must be several times less than assumed here (in order to be consistent with the observed total iron abundance), which is unlikely since the iron production per SNIa is constrained by light curve energetics. Given the IMF assumed above, if the SNIa formation efficiencies are in the range used here, then the CSFR would have to be an order of magnitude larger than we derive from the DSNB. The additional light generated from the increase in intermediate mass and core-collapse mass stars would exceed the measurements discussed here and, in addition, 90% of massive stars must be neutrino-impotent in order to not be observed by Super-Kamiokande, an unlikely scenario (see Section 7.2). These considerations lead us to conclude that SNIa do not significantly contribute to the MeV CGB.

If the CGB is not due to SNIa, then what? In Figure 4 we show three possible sources of to the CGB: Seyferts, SNIa, and a somewhat arbitrary extrapolation of the  $> 10$  MeV background (as measured by COMPTEL and EGRET) [24]. In combination, this three-component model seems to be a reasonable fit to the CGB with the dominant contribution at MeV energies arising from a newly postulated source: MeV Blazars, by which we mean objects with emission spectra similar to the Blazars thought to generate

the  $> 10$  MeV CGB, but now with numbers and distribution sufficient to account for the observed MeV CGB intensity [72]. We note that the Blazars required to generate the  $> 10$  MeV CGB are expected to be cut off below  $\sim 5$  MeV and the sources required to make the  $\sim 1$  MeV CGB have yet to be observed. Such MeV Blazars, or additional astrophysical sources, will be further tested by future gamma ray telescopes (e.g., ACT, MEGA, and NCT [78–80]).

Additionally, we can consider models for new physics which predict or allow contributions to the present-day MeV CGB, for example the decay of non-baryonic cold dark matter [81–89], the decay of massive gravitons predicted by models of extra dimensions [90–94], and primordial black hole evaporation [95–97]. Photons from these sources may have a featureless energy spectrum which is isotropic on the sky, and which could be distinguished from candidate astrophysical sources by the angular correlations [28]. The uncertain origin of the MeV CGB opens up a new window for these studies.

### 7.2. Implications for Failed Supernovae

In our analysis, we have used observables and limits which probe the star formation rate at different stages of stellar evolution. The UV, optical, and IR observations probe the massive CSFR *before* the neutrino emission from core-collapse, while the optical measurements of the supernova rates and the heavy metal abundances probe the CSFR *after* the neutrino emission. The optical determinations of the supernova rates are particularly important. A measurement of the ratio of the optical SNII to the SNIa rate in the ranges determined in Figure 3 implies that most SNII are optically successful, with no significant failure rate due to prompt black hole formation (after most of the neutrinos are emitted) [19–21]. Good agreement between these *before* and *after* observations, combined with the results from SN 1987A, imply that there would be no astrophysical mechanism which can suppress the DSNB flux. Novel neutrino properties, e.g., invisible decays, could deplete the fluxes from astrophysical neutrinos [98–100], and Ando [101] and Fogli et al. [102] have considered the effects on the DSNB in detail.

This result is of high importance for the current detection of the DSNB flux. With robust measurements of the optical SNII rate, the DSNB flux could be predicted with no model dependence from the CSFR or IMF. This should be an important priority for astronomical observations. Given the few direct measurements for the optical SNII rate, however, the DSNB flux is presently the most stringent limit on the core-collapse and optical SNII rate. With a core-collapse rate derived from the CSFR, a measurement of the DSNB flux by itself can determine the fraction of massive core-collapse events which fail to emit neutrinos. With the optical data as well, the DSNB flux would also be the most robust measurement of the fraction of core-collapse events which fail to explode as optical SNII.

### 7.3. Detection of the Diffuse Supernova Neutrino Background

As we have discussed above, all indications from the CSFR observations are that the DSNB flux *is* on the verge of detection, which has been re-substantiated by the recent results from GALEX [33], for which the best fit CSFR predicts a nearly detectable DSNB. Note that dust corrections larger than indicated in Figure 1 would begin to present a serious inconsistency with the neutrino data. The current configuration of Super-Kamiokande gives the best detection potential for the flux through the  $\bar{\nu}_e$  channel, though currently this search is limited to the exponential tail of the spectrum at energies greater than 19.3 MeV. Loading Super-Kamiokande with gadolinium trichloride would allow tagging of neutron captures, significantly lowering backgrounds and the analysis threshold [36]. This would allow a quick detection of the DSNB, and is the only realistic possibility for measuring the DSNB spectrum shape [36]. Detection of the DSNB flux will be important for studying the supernova rates, and could also be an exciting milestone discovery of the first astrophysical source of neutrinos beyond the Sun and SN 1987A.

## 8. Acknowledgments

We thank Shin'ichiro Ando, Dieter Hartmann, Manoj Kaplinghat, and Mark Leising for discussions. J.F.B. was supported by The Ohio State University, and L.E.S. and T.P.W. were supported at OSU by the Department of Energy grant DE-FG02-91ER40690. P.Z. was supported by the DOE and the NASA grant NAG 5-10842 at Fermilab.

## 9. References

- [1] Gallego J, Zamorano J, Aragon-Salamanca A Rego M, 1995 *Astrophys. J. Lett.* **455** 1
- [2] Lilly S J, Le Fevre O, Hammer F and Crampton D, 1996 *Astrophys. J. Lett.* **460** 1
- [3] Steidel C C, Giavalisco M, Pettini M, Dickinson M and Adelberger K L, 1996 *Astrophys. J. Lett.* **462** 17
- [4] Connolly A J, Szalay A S, Dickinson M, Subbarao M U and Brunner R J 1997 *Astrophys. J. Lett.* **486** 11
- [5] Cowie L, Songaila A and Barger A J, 1999 *Astron. J.* **117** 2656
- [6] Sullivan M, et al., 2000 *Mon. Not. R. Astron. Soc.* **312** 442
- [7] Scott S, Fox M, Dunlop J S, et al., 2002 *Mon. Not. R. Astron. Soc.* **331** 817
- [8] Chapman S C, Blain A W, Ivison R J and Smail I R, 2003 *Nature* **422** 695
- [9] Ouchi M et al., 2004 *Astrophys. J.* **611** 685
- [10] Stanway E R, Bunker A J, and McMahan R G 2003 *Mon. Not. R. Astron. Soc.* **342** 439
- [11] Heavens A, Panter B, Jimenez R and Dunlop J, 2004 *Nature* **428** 625
- [12] Hirata K et al., 1987 *Phys. Rev. Lett.* **58** 1490
- [13] Bionta R M et al., 1987 *Phys. Rev. Lett.* **58** 1494
- [14] Ando S, Beacom J F and Yuksel H, astro-ph/0503321
- [15] Malek M et al., 2003 *Phys. Rev. Lett.* **90** 061101
- [16] Ando S, Sato K and Totani T, 2003 *Astropart. Phys.* **18** 307
- [17] Fukugita M and Kawasaki M, 2003 *Mon. Not. Roy. Astron. Soc.* **340** L7
- [18] Strigari L E, Kaplinghat M, Steigman G and Walker T P, 2004 *JCAP* **0403** 007
- [19] Heger A, Fryer C L, Woosley S E, Langer N and Hartmann D H, 2003 *Astrophys. J.* **591** 288



- [20] Beacom J F, Boyd R N and Mezzacappa A, 2000 Phys. Rev. Lett. **85** 3568
- [21] Beacom J F, Boyd R N and Mezzacappa A, 2001 Phys. Rev. D **63** 073011
- [22] Hauser M G and Dwek E, 2001 Ann. Rev. Astron. Astrophys. **39** 249
- [23] Wright E L, 2004 New Astron. Rev. **48** 465
- [24] Sreekumar P, Stecker F W and Kappadath S C, 2004 AIP Conf. Proc. **510** 459
- [25] Clayton D and The L-S, 1991 Astrophys. J. **375** 221
- [26] Watanabe K, Hartmann D H, Leising M D and The L-S, 1999 Astrophys. J. **516** 285
- [27] Ruiz-Lapuente P, Casse M and Vangioni-Flam E, 2001 Astrophys. J. **549** 483
- [28] Zhang P J and Beacom J F, 2004 Astrophys. J. **614** 37
- [29] Tresse L, Maddox S J, Le Fevre O and Cuby J G, 2002 Mon. Not. Roy. Astron. Soc. **337** 369
- [30] Glazebrook K et al., 2003 Astrophys. J. **587** 55
- [31] Baldry I K and Glazebrook K, 2003 Astrophys. J. **593** 258
- [32] Dahlen T et al., 2004 Astrophys. J. **613** 189
- [33] Schiminovich D et al., 2005 Astrophys. J. **619** L47
- [34] Cole S et al., 2001 Mon. Not. R. Astron. Soc. **326** 255
- [35] Strolger L G et al., 2004 Astrophys. J. **613** 200
- [36] Beacom J F and Vagins M R, 2004 Phys. Rev. Lett. **93** 171101
- [37] Bisnovatyi-Kogan G S and Seidov Z F, 1984 Sov. Astron. **26** 132
- [38] Krauss L M, Glashow S L and Schramm D N, 1984 Nature **310** 191
- [39] Dar A, 1985 Phys. Rev. Lett. **55** 1422
- [40] Woosley S E, Wilson J R and Mayle R, 1986 Astrophys. J. **302** 19
- [41] Totsuka Y, 1992 Rep. Prog. Phys. **55** 377
- [42] Totani T and Sato K, 1995 Astropart. Phys. **3** 367
- [43] Totani T, Sato K and Yoshii Y, 1996 Astrophys. J. **460** 303
- [44] Malaney R A, 1997 Astropart. Phys. **7** 125
- [45] Hartmann D H and Woosley S E, 1997 Astropart. Phys. **7** 137
- [46] Kaplinghat M, Steigman G and Walker T P, 2000 Phys. Rev. D **62** 043001
- [47] Ando S and Sato K, 2003 Phys. Lett. B **559** 113
- [48] Ando S and Sato K, 2004 New J. Phys. **6** 170
- [49] Turner M, 2002 Int. J. Mod. Phys. **A17** 3446
- [50] Keil M T, Raffelt G G and Janka H T, 2003 Astrophys. J. **590** 971
- [51] Baldry I K and Glazebrook K, 2003 Astron. J. **126** 1483
- [52] Madau P, Della Valle M D and Panagia N, 1998 Mon. Not. R. Astron. Soc. **297** L17
- [53] Gal-Yam A and Maoz D, 2004 Mon. Not. Roy. Astron. Soc. **347** 942
- [54] Maoz D and Gal-Yam A, 2004 Mon. Not. Roy. Astron. Soc. **347** 951
- [55] Yoshii Y, Tsujimoto T and Nomoto K, 1996 Astrophys. J. **462** 266
- [56] Blanc G et al., 2004 Astron. and Astrophys. **423** 881
- [57] Cappellaro E et al, 2005 Astron. and Astrophys. **430** 83
- [58] M Hamuy, (2003) in Core Collapse of Massive Stars, ed. C.L. Fryer (Dordrecht: Kluwar), astro-ph/0301006
- [59] A Renzini, in Clusters of Galaxies: Probes of Cosmological Structure and Galaxy Evolution, ed. J S Mulchaey, A Dressler, and A Oemler (Cambridge: Cambridge Univ. Press), astro-ph/0307146
- [60] Prochaska J X, Gawiser E, Wolfe A M, Castro S and Djorgovski S G, 2003 Astrophys. J. **595** L9
- [61] Anders E and Grevesse N, 1989 Geochim. Cosmochim. Acta **53** 197
- [62] Norman C et al., 2004 Astrophys. J. **607** 721
- [63] Loeb A and Haiman Z, 1997 Astrophys. J. **490** 571
- [64] <http://www.spitzer.caltech.edu/index.shtml>
- [65] Hartmann D H, Watanabe K, Leising M D, The L-S and Woosley S E 1997, in the proceedings of the Fourth Compton Symposium, eds. C. D. Dermer, M. S. Strickman, and J. D. Kurfess, Williamsburg VA April 1997, AIP Proc. No. 410, p 1228.
- [66] Buonanno A, Sigl G, Raffelt G G, Janka H T and Muller E, astro-ph/0412277.

- [67] Watanabe K, Leising M D, Share G H and Kinzer R L, in The Fifth Compton Symposium, ed. M L McConnell and J M Ryan 2000
- [68] Weidenspointner G et al., in The Fifth Compton Symposium, ed. M L McConnell and J M Ryan 2000
- [69] Kappadath S C, 1998, PhD. Thesis, Univ. of New Hampshire
- [70] Watanabe K and Hartmann D, in Gamma-ray Astrophysics 2001, Baltimore, Maryland, 4-6 April 2001 Editors, S Ritz, N Gehrels, C R Shrader
- [71] Stecker F and Salamon M H, *ibid* pp. 432-441
- [72] Blom J J et al., 1995 *Astron. and Astrophys.* **298** L33
- [73] Kinzer R L et al., 1997 *Astrophys. J.* **475** 361
- [74] Sreekumar P et al., 1998 *Astrophys. J.* 494 523
- [75] Zdziarski A A, 1996 *Mon. Not. R. Astron. Soc.* **281** L9
- [76] Nomoto K, Thielemann F K and Yokoi K, 1984 *Astrophys. J.* **286** 644
- [77] Milne A et al., astro-ph/0406173
- [78] Milne P A, Kroeger R A, Kurfess J D and The, L-S 2002 *New Astronomy Review* **46** 617
- [79] Bloser P F, Andritschke R, Kanbach G, Schoenfelder V, Schopper F and Zoglauer A, 2002 *New Astron. Rev.* **46** 611
- [80] <http://ssl.berkeley.edu/gamma/nct.html>
- [81] Kamionkowski M, 1994, astro-ph/9404079
- [82] Barbieri R and Berezhinsky V, 1988 *Physics Letters B* **205** 559
- [83] Gondolo P, 1992 *Physics Letters B* **295** 104
- [84] Ellis J, Gelmini G B, Lopez J L, Nanopoulos D V and Sarkar S, 1992 *Nuclear Physics B* **373** 399
- [85] Kribs G D and Rothstein I Z, 1997 *Phys. Rev. D* **55** 4435; *ibid* **56** 1822
- [86] Chen X and Kamionkowski M, 2004 *Phys. Rev. D* **70** 43502
- [87] Abazajian K, Fuller G M and Patel M, 2001 *Phys. Rev. D* **64** 023501
- [88] Feng J L, Rajaraman A and Takayama F, 2003 *Phys. Rev. D* **68** 063504
- [89] Olive K A and Silk J, 1985 *Phys. Rev. Lett.* **55** 2362
- [90] Arkani-Hamed N, Dimopoulos S and Dvali G, 1999 *Phys. Rev. D* **59** 086004
- [91] Hall L J and Smith D, 1999 *Phys. Rev. D* **60** 085008
- [92] Hannestad S and Raffelt G G, 2003 *Phys. Rev. D* **67** 125008
- [93] Casse M, Paul J, Bertone G and Sigl G, 2004 *Phys. Rev. Lett.* **92** 111102
- [94] Kolb E W, Servant G and Tait T M P, 2003 *J. Cosmo. and Astropart. Phys.* **7** 8
- [95] Kim H I, Lee C H and MacGibbon J H, 1999 *Phys. Rev. D* **59** 063004
- [96] Daghigh R and Kapusta J, 2002 *Phys. Rev. D* **65** 064028
- [97] Sendouda Y, Nagataki S and Sato K, 2003 *Phys. Rev. D* **68** 103510
- [98] Beacom J F and Bell N F, 2002 *Phys. Rev. D* **65** 113009
- [99] Beacom J F, Bell N F, Hooper D, Pakvasa S and Weiler T J, 2003 *Phys. Rev. Lett.* **90** 181301
- [100] Beacom J F, Bell N F, Hooper D, Pakvasa S and Weiler T J, 2003 *Phys. Rev. D* **68** 093005
- [101] Ando S, 2003 *Phys. Lett. B* **570** 11
- [102] Fogli G L, Lisi E, Mirizzi A and Montanino D, 2004 *Phys. Rev. D* **70** 013001